

Emergent Fermi surface in a triangular-lattice SU(4) quantum antiferromagnet

Anna Keselman,¹ Bela Bauer,² Cenke Xu,³ and Chao-Ming Jian²

¹*Kavli Institute for Theoretical Physics, University of California, Santa Barbara, CA 93106-4030*

²*Microsoft Station Q, Santa Barbara, California 93106-6105, USA*

³*Department of Physics, University of California, Santa Barbara, CA 93106, USA*

Motivated by multiple possible physical realizations, we study the SU(4) quantum antiferromagnet with a fundamental representation on each site of the triangular lattice. We provide evidence for a gapless liquid ground state of this system with an emergent Fermi surface of fractionalized fermionic partons coupled with a U(1) gauge field. Our conclusions are based on numerical simulations using the density matrix renormalization group (DMRG) method, which we support with a field theory analysis.

PACS numbers:

Realizations of quantum spin liquids — quantum phases of spins whose ground state is not described by local ordering patterns but instead characterized by exotic quantum entanglement — have been highly sought-after since such phase was first hypothesized [1]. Within the broad family of spin liquids, a particularly elusive category are gapless spin liquids that exhibit gapless excitations on an extended region in the momentum space, akin to the Fermi surface in ordinary metals. The known realizations of such gapless phases in systems of SU(2) spins usually require complicated Hamiltonians beyond the Heisenberg interaction, such as ring exchange terms [2–9], staggered chiral three-spin interactions [10, 11], or antiferromagnetic Kitaev interactions in an external field [12–14].

Here, we report strong evidence for a gapless liquid with an emergent Fermi surface of fractionalized partons in the nearest-neighbor SU(4) Heisenberg quantum antiferromagnet on the triangular lattice with a fundamental representation on each site. While SU(N) antiferromagnets were suspected to harbor exotic phases already in the early days of the field [15–21] and recent work has demonstrated the presence of a Dirac spin liquid in the same model on the honeycomb lattice [22], our motivation for studying this model stems primarily from the availability of several possible experimental realizations. In transition metal oxides, spin and orbital degrees of freedom may be described by an effective SU(4) quantum magnet [23–25]. Cold atomic gases formed by atoms with large hyperfine spin component can form effective SU(N) quantum antiferromagnet [26], and spin-3/2 atoms can naturally form Sp(4) or SU(4) quantum antiferromagnet [27–29] when only the s -wave scattering between the atoms is considered. Most recently, it was also proposed that some of the $2d$ systems with Moiré superlattices may be described by an approximate SU(4) quantum antiferromagnet [30–34] at commensurate fillings where correlated insulators were observed recently [35–37].

In the following, we will first introduce a parton mean-field construction for a candidate liquid state for the model. We then carefully examine the properties of this state when placed on quasi-one-dimensional cylin-

der geometries, including the effects of symmetry-allowed perturbations specific to these geometries. These will also be the target of unbiased numerical simulations using the density-matrix renormalization group (DMRG) method [38, 39]. We find our numerical results to be in agreement with predictions from the field theory that describes the proposed liquid state. For two cases of even circumference, we find gapped states with ordering patterns which are consistent with the one-dimensional field theory that contains relevant symmetry-allowed perturbations deviating from a gapless fixed point; while in a case with odd circumference, where there are no relevant translation-symmetric operators, we find a gapless state whose structure factor exhibits sharp features consistent with the field theory. We thus conclude that our proposed theory describes the system accurately in quasi-one-dimensional geometries and thus likely also in the two-dimensional limit.

Model- We study the Kugel-Khomskii model [40] on the two-dimensional triangular lattice at the SU(4) symmetric point

$$H = J \sum_{\langle ij \rangle} \left(2\mathbf{S}_i \cdot \mathbf{S}_j + \frac{1}{2} \right) \left(2\mathbf{V}_i \cdot \mathbf{V}_j + \frac{1}{2} \right), \quad (1)$$

where $J > 0$ is an antiferromagnetic coupling, and \mathbf{S}_i (\mathbf{V}_i) denote the $S = 1/2$ spin (orbital) degrees of freedom at site i . We denote the three Pauli matrices that act on the two-fold spin (orbital) indices as σ^a (τ^a), such that $S^a = \sigma^a/2$ ($V^a = \tau^a/2$) with $a = x, y, z$. We can view the degrees of freedom on each site as a pseudospin in the fundamental representation of SU(4), with the 15 operators $\{\sigma^a, \tau^b, \sigma^a \tau^b\}_{a,b=x,y,z}$ being the 15 generators of SU(4). The Hamiltonian Eq. (1) can be interpreted as an SU(4) antiferromagnetic Heisenberg model.

The Hamiltonian Eq. (1) is invariant under the global SU(4) pseudospin rotation symmetry, as well as the spatial symmetries of the triangular lattice including the translation symmetries $T_{1,2}$, the mirror symmetry \mathcal{M} and the 6-fold rotation symmetry C_6 as shown in Fig. 1(a). In addition, as a spin-orbital system, the model naturally admits a time-reversal (TR) symmetry \mathcal{T} whose action depends on the physical nature of the orbital degrees of

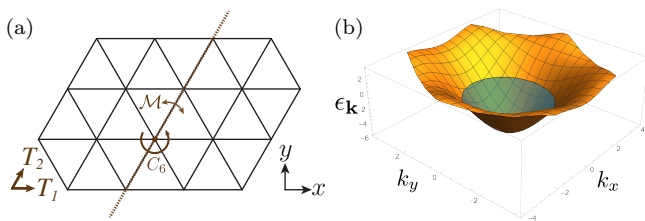


FIG. 1: (a) T_1 and T_2 denote the translation symmetries along the two basis vectors of the 2d triangular lattice. \mathcal{M} denotes the mirror symmetry with the T_2 direction as the mirror plane and C_6 denotes the 6-fold crystal rotation symmetry. (b) The parton mean-field band structure (orange), i.e. the single parton energy $\epsilon_{\mathbf{k}}$ as a function of crystal momentum $k_{x,y}$, is shown. The Fermi level corresponding to filling $\nu = 1/4$ is depicted in blue.

freedom. If the orbital space is the valley space in the Moiré systems where the valleys are exchanged under the TR symmetry, \mathcal{T} acts on the SU(4) pseudospin degrees of freedom as the operator $i\sigma^y\tau^x\mathcal{K}$ with \mathcal{K} representing the complex conjugation. In systems where the orbitals transform trivially under \mathcal{T} , the TR action is given by the operator $i\sigma^y\mathcal{K}$ instead. As we will see, all our discussions below apply to both realizations of the TR symmetry.

Fermionic parton mean-field ansatz- We now construct a candidate for the ground state of the model in Eq. (1). We start by introducing a 4-component fermionic parton on each site, and use $f_{i,m=1,\dots,4}$ (and $f_{i,m}^\dagger$) to denote the corresponding annihilation (and creation) operators. The four components of the fermionic parton can be also labeled by the two-fold spin indices and two-fold orbital indices. They transform into each other under the global SU(4) pseudospin rotation. The SU(4) pseudospin operators (on the site i) can be represented in terms of the fermionic parton as

$$S_i^a = \frac{1}{2}f_{i,m}^\dagger\sigma^a f_i, \quad V_i^b = \frac{1}{2}f_{i,m}^\dagger\tau^b f_i, \quad (S^a V^b)_i = \frac{1}{4}f_{i,m}^\dagger\sigma^a\tau^b f_i. \quad (2)$$

The physical Hilbert space of SU(4) pseudospins is obtained from the Hilbert space of the fermionic partons by imposing the constraint $n_i = \sum_{m=1}^4 f_{i,m}^\dagger f_{i,m} = 1$ on each site i .

We consider the simplest parton mean-field ansatz given by the following mean-field Hamiltonian:

$$H_{\text{mf}} = -t \sum_{\langle ij \rangle} \sum_{m=1}^4 f_{i,m}^\dagger f_{j,m} + h.c. \quad (3)$$

which only contains nearest-neighbor parton hoppings with a uniform $t > 0$ on the triangular lattice. This mean-field ansatz preserves the full SU(4) pseudospin rotation symmetry, the space-group symmetries of the triangular lattice, and the time-reversal symmetry \mathcal{T} that transforms the partons as $f_i \rightarrow i\sigma^y\tau^x f_i$ when the orbitals

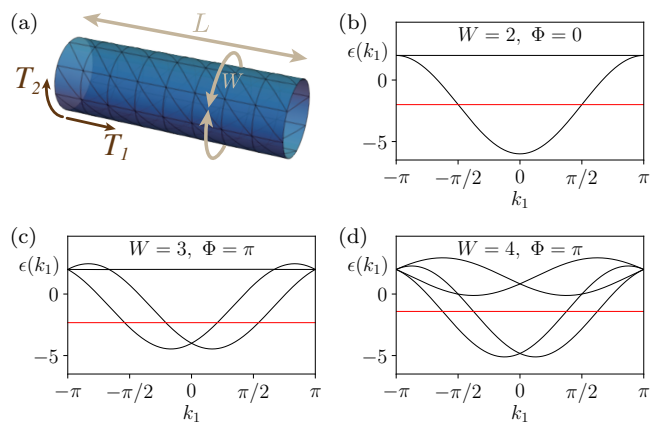


FIG. 2: (a) Compactification of the 2d lattice along the T_2 direction, resulting in a cylinder geometry. (b,c,d) The parton mean-field band structure (with energies given in the unit of t) on the compactified, quasi-1d geometry, when the number of unit cells along T_2 is $W=2,3,4$, respectively. In this geometry an additional degree of freedom, the flux Φ through the cylinder has to be considered. We plot the band structure for a flux of $\Phi = 0$ for $W = 2$, and $\Phi = \pi$ for $W = 3, 4$.

are physically realized by valleys and as $f_i \rightarrow i\sigma^y f_i$ when the orbitals transform trivially under \mathcal{T} .

This mean-field ansatz yields a single 4-fold-degenerate parton band. At the mean-field level, the single-occupancy constraint $n_i = 1$, requires the partons have filling factor $\nu = 1/4$ and hence, results in a parton Fermi surface as shown in Fig. 1(b). Beyond mean-field, the constraint above can be implemented by a dynamical U(1) gauge field coupled to the fermionic partons.

Finite circumference cylinders- Our numerical simulations will be performed for cylinder geometries that are constructed by compactifying the T_2 direction and imposing periodic boundary conditions on the SU(4) pseudospin variables (see Fig. 2(a)). The circumference of the cylinder is denoted as W and the length (along the T_1 direction) of the cylinder as L . The quasi-1d system with finite W (and infinite L) maintains the space-group symmetry $T_{1,2}$ and \mathcal{M} but breaks the C_6 symmetry to a two-fold crystal rotation symmetry C_2 .

We can place the mean-field Hamiltonian (3) on the same geometry if we additionally specify the boundary condition for the partons in the T_2 direction. The only choices that preserve either one of the TR symmetry or the product of mirror and rotation $\mathcal{M}C_2$ are periodic and antiperiodic boundary conditions. These can also be interpreted as placing a U(1) gauge flux $\Phi = 0$ and $\Phi = \pi$, respectively, through the cylinder. In general, there isn't a simple reasoning which value of Φ is more favorable for a certain geometry. We can view it as a discrete parameter (our only parameter) when comparing the parton ansatz and the results of the DMRG study.

For finite W , the two-dimensional parton band structure reduces to W (4-fold degenerate) one-dimensional

bands, each parameterized by the crystal momentum k_1 along the T_1 direction. Different one-dimensional bands can be distinguished by their crystal momentum k_2 along the T_2 direction. The parton Fermi level is still determined by the parton filling constraint $\nu = 1/4$. In general, the number of (partially) occupied one-dimensional parton bands depends on both W and Φ . In the following, we will focus on the $\Phi = 0$ scenario for $W = 2$ and $\Phi = \pi$ for $W = 3, 4$, as we find that these choices are most consistent with the DMRG results. The corresponding one-dimensional band structures are shown in Fig. 2(b-d). A more comprehensive comparison with different choices of Φ for $W = 2, 3, 4$ is given in the Supplementary Material [41]. The Fermi momenta for each W can be calculated directly from the mean-field Hamiltonian Eq. (3). For $W = 2$ with $\Phi = 0$, the single partially occupied band has $k_2 = 0$ and the k_1 -values of the Fermi momenta are $\pm\pi/2$. For $W = 3, 4$ with $\Phi = \pi$, the two bands that are (partially) occupied by the partons have crystal momenta $k_2 = \pm\pi/W$ and the k_1 -values of the four Fermi momenta are $\pm\pi/(2W) \pm \pi W/8$. In fact, in all the cases we consider, these Fermi momenta are also completely fixed by the symmetries, as we show in detail in the Supplementary Material [41]. Pairwise differences of the Fermi momenta will play an important role in the later discussion.

For each W , by linearizing the parton band structure around each Fermi point, we can write down a continuum Lagrangian of low-energy partons in these quasi-1d geometries:

$$\mathcal{L}_W^{(0)} = \sum_{r,n,m} [\psi_{r,n,m}^\dagger (i\partial_0 + v_r i\partial_1) \psi_{r,n,m}]. \quad (4)$$

Here $\mu = 0, 1$ label the temporal and spatial components. The fermionic fields $\psi_{r,n,m}$ describe the low-energy partons near the Fermi points, where m is the SU(4) pseudospin index, n is the band index, and $r = R(L)$ stands for right(left) movers with a velocity $v_{r,n} = \pm v_n$ respectively. In all the scenarios we consider, the Fermi points in a given geometry are all related by symmetries (\mathcal{T} , \mathcal{M} and C_2), so are the respective velocities. Thus, we find that the Lagrangian in Eq. (4) describes SU(4)-invariant massless Dirac fermions for $W = 2$, whereas for $W = 3, 4$ it describes massless Dirac fermions with an enhanced SU(8) symmetry.

Going beyond the mean-field level, the parton filling constraint, $n_i = 1$, leads to the coupling of the low-energy fermions in Eq. (4) to a dynamical U(1) gauge field a_μ , via the substitution $i\partial_\mu \rightarrow i\partial_\mu - a_\mu$. Thus, the low-energy theory for $W = 2$ ($W = 3, 4$) is given by the $N_f = 4$ ($N_f = 8$) QED₂, or equivalently the 1+1d SU(4)₁ (SU(8)₁) conformal field theory (CFT), whose energy spectrum is gapless. The Dirac mass terms are forbidden in all of these cases due to the translation symmetry T_1 .

We next consider symmetry-allowed relevant perturbations to these gapless theories. More specifically, we will focus on possible Umklapp scatterings for each W . Al-

though these perturbations are not expected to appear in the 2d limit, we will see that they can change the low-energy physics dramatically for the cases with finite circumferences we study numerically.

For $W = 2$, the distance between the two Fermi points allows for the following symmetry-preserving Umklapp interaction

$$\mathcal{L}_{W=2,\Phi=0}^{\text{int}} = \left(\sum_{m=1}^4 \psi_{L,m}^\dagger \psi_{R,m} \right)^2 + h.c., \quad (5)$$

where we suppressed the band index in the fields $\psi_{L,m}^\dagger$ and $\psi_{R,m}$ because there is only one (partially) occupied band. This interaction commutes with T_1 because the Fermi momenta dictate that under T_1 , $\psi_{L,m} \rightarrow e^{-i\pi/2} \psi_{L,m}$, $\psi_{R,m} \rightarrow e^{i\pi/2} \psi_{R,m}$. Using the Fierz identity, this Umklapp interaction can be written as a back-scattering between left-moving and right-moving primary fields in the SU(4)₁ CFT, both carrying the 6-dimensional representation of SU(4) (see Supplementary Material [41] for more details). In the SU(4)₁ CFT, each of such primary fields has scaling dimension 1/2. Therefore, the Umklapp interaction has a scaling dimension 1 and, hence, is a relevant perturbation. It can lead to a phase with a finite vacuum expectation value $\langle \sum_{m=1}^4 \psi_{L,m}^\dagger \psi_{R,m} \rangle$ that gaps out all low-energy degrees of freedom and spontaneously breaks the T_1 -translation symmetry by doubling the unit cell in the T_1 direction. Other symmetries stay intact in this gapped phase. In fact, for $W = 2$, doubling of the unit cell along the T_1 direction in a gapped phase is expected due to the 1d Lieb-Schultz-Mattis constraint for SU(4) spin chains [42].

For $W = 3$, due to the (relative) positions of the Fermi points, the symmetry-allowed Umklapp terms are of high orders (i.e. at least 16) in terms of the low-energy fermion fields. Therefore, the effect of Umklapp terms here can be neglected, and the SU(8)₁ CFT (or equivalently the $N_f = 8$ QED₂) remains a good description of the system. With $W = 3$, each unit cell in the T_1 direction has three SU(4) pseudospins. In the absence of T_1 symmetry breaking, the system has to be gapless based on the SU(4) Lieb-Schultz-Mattis constraint [42].

For $W = 4$, the (relative) positions of the Fermi points allow for the following symmetry-preserving Umklapp interactions

$$\left(\sum_m \psi_{L,n,m}^\dagger \psi_{R,n,m} \right) \left(\sum_m \psi_{L,n',m}^\dagger \psi_{R,n',m} \right) + h.c., \quad (6)$$

where $n, n' = 1, 2$ label the two 1d parton bands that are (partially) occupied. Again these interactions preserve the translation T_1 , as its action is given by $T_1 : \sum_m \psi_{L,n,m}^\dagger \psi_{R,n,m} \rightarrow -\sum_m \psi_{L,n,m}^\dagger \psi_{R,n,m}$ for $n = 1, 2$. These Umklapp interactions can all be written as the back-scattering between left-moving and right-moving primary fields in the SU(8)₁ CFT which both carry the 28-dimensional representation of SU(8) (see Supplementary Material [41] for more details). In the SU(8)₁ CFT,

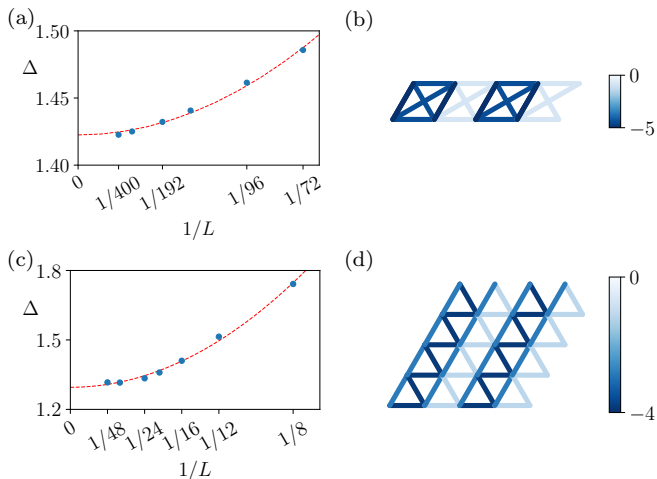


FIG. 3: (a,c) Pseudospin gap as function of inverse system size for finite cylinders of width $W = 2, 4$ obtained using a bond dimension of up to $M = 4000$, resulting in truncation errors of $\epsilon_{\text{tr}} \simeq 10^{-5}$ ($\epsilon_{\text{tr}} \simeq 10^{-9}$) for $W = 4$ ($W = 2$). Red dashed line in each of the plots is a fit to $\Delta_0 + a/L^2$ yielding $\Delta_0 = 1.42$ for $W = 2$ and $\Delta_0 = 1.29$ for $W = 4$. (b,d) The bond expectation values for the middle four rungs in a cylinder of length $L = 24$ and width $W = 2, 4$ respectively.

each of such primary fields has a scaling dimension $3/4$. Therefore, each of these Umklapp interactions has a scaling dimension $3/2$ and again is a relevant perturbation. These perturbations can lead to a phase with nonzero expectation value of $\langle \sum_{m=1}^4 \psi_{L,n,m}^\dagger \psi_{R,n,m} \rangle$ (for both $n = 1, 2$) that gap out the system while breaking the T_1 -translation symmetry by doubling the unit cell. Other symmetries remain intact in this gapped phase. Interestingly, for $W = 4$, each unit cell along the T_1 has four SU(4) pseudospins. Thus, in this case, the SU(4) Lieb-Schultz-Mattis constraint does not require a gapped phase to break the T_1 translation symmetry. As we will demonstrate, the DMRG with $W = 4$ also shows a doubling of the unit cell, which is consistent with our field theory analysis.

Numerical study- We perform DMRG simulations using the ITensor library [43]; to accelerate the simulations, we explicitly conserve three U(1) quantum numbers corresponding to total S^z , V^z , and $S^z V^z$. A key observable is the pseudospin gap Δ , which we obtain as the energy difference between the ground states in the sectors with $(S^z, V^z, S^z V^z) = (0, 0, 0)$ (which contains the SU(4) singlet) and $(S^z, V^z, S^z V^z) = (1, 0, -1/2)$. For each cylinder circumference W , we obtain the gap Δ for cylinders of varying length and then perform an extrapolation to the thermodynamic limit.

The gap obtained for $W = 2, 4$ is shown in Fig. 3(a,c). In both cases, we find that the gap remains finite in the limit of $L \rightarrow \infty$, consistent with the expectation of a gapped phase due to the Umklapp scattering. Translation-symmetry breaking can be observed directly in the bond expectation values $\langle \sum_{\alpha} \mathcal{S}_i^{\alpha} \cdot$

$\mathcal{S}_j^{\alpha} \rangle$, where \mathcal{S}^{α} are the 15 SU(4) pseudospin operators $\{\sigma^a, \tau^b, \sigma^a \tau^b\}_{a,b=x,y,z}$, and i, j are a pair of nearest-neighbor sites. The pattern of bond expectation values is shown for the middle four rungs in a cylinder of length $L = 24$ and circumference $W = 2, 4$ in Fig. 3(b,d). In both cases one can clearly see that the translation symmetry is broken and there is a unit cell doubling along T_1 , in agreement with the symmetry-breaking pattern expected from the field theory analysis in the previous section. We emphasize that for $W = 4$, no translation symmetry breaking along the circumference of the cylinder (i.e., along T_2) is observed (see Supplementary Material [41] for more details), indicating that the state does not originate from plaquette coverings of the lattice as proposed in Refs. 21, 44.

The finite-size behavior of the gap for $W = 3$ is shown in Fig. 4(a). Although the results for the gap are not fully conclusive, they are consistent with either a vanishing or a very small gap. Here, a bond dimension of up to $M = 8000$ was used, resulting in a truncation error of $\epsilon_{\text{tr}} \simeq 5 \cdot 10^{-5}$ for the ground state. Since the truncation errors in the $S^z = 1$ sector were slightly higher, to obtain a more accurate value for the gap we performed an extrapolation of the energy with truncation error in each sector before subtracting the two (see Supplementary Material [41] for further details).

To understand the nature of the state in this case, we consider the static SU(4)-pseudospin structure factor,

$$\mathcal{F}(\vec{k}) = \sum_i e^{i\vec{k} \cdot (\vec{r}_i - \vec{r}_{i_0})} \sum_{\alpha} \langle \mathcal{S}_i^{\alpha} \cdot \mathcal{S}_{i_0}^{\alpha} \rangle, \quad (7)$$

where \vec{r}_i, \vec{r}_{i_0} denote the positions of the sites i, i_0 . For a gapless state with a parton Fermi surface, the structure factor is expected to exhibit cusps at particular momenta corresponding to the “ $2k_F$ ” values of the Fermi sea. Fig. 4(c) shows the structure factor calculated in the ground state of a length $L = 32$ cylinder using DMRG. Comparing it to the structure factor calculated for the mean-field ansatz with $\Phi = \pi$ using Wick’s theorem (Fig. 4(b)), we observe good qualitative agreement and in particular see that the cusps appear at the same momenta.

Finally, we note that starting from the mean-field ansatz, the coupling to the gauge field may be numerically implemented by a Gutzwiller projection, i.e. projecting the mean-field wavefunction to a single-occupancy on each site. The correlations in the resulting state can be probed using Monte Carlo sampling of the projected wavefunction. Carrying out this projection, we find that although we do not observe any symmetry breaking for $W = 2, 4$, the power-law decay of the SU(4) pseudospin correlation function $\sum_{\alpha} \langle \mathcal{S}_i^{\alpha} \cdot \mathcal{S}_{i_0}^{\alpha} \rangle$ in both cases agrees with the CFT prediction. This result suggests that the Gutzwiller projection does not capture the effect of the Umklapp interactions which are particularly important to the cylinder geometries with $W = 2, 4$. For $W = 3$, we verify that the cusps in the structure factor remain at the same position in the momentum space as for the

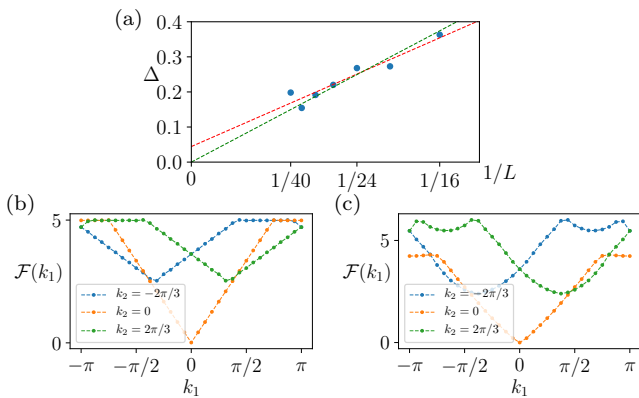


FIG. 4: (a) Pseudospin gap as function of inverse system size for finite cylinders of circumference $W = 3$. Red dashed line is a linear fit, while the green dashed line is a fit to $\Delta = a/L$. We note that the value of the gap for the largest system size of $L = 40$ is less reliable, as the energy extrapolation procedure is less accurate for this system size. (b,c) Pseudospin structure factor obtained for a finite cylinder with $W = 3$ and length $L = 32$ with respect to a site in the middle of the system. (b) Non-interacting partons in the mean-field band structure with $\Phi = \pi$; (c) DMRG.

mean-field ansatz. Further details and numerical results are given in the Supplementary Material [41].

Discussion- For the quasi-1d geometries with $W = 2, 3, 4$, the DMRG results agree well with the analysis based on the parton mean-field ansatz plus possible Umklapp interactions. We emphasize that the symmetry-allowed Umklapp interactions considered are all partic-

ular to certain geometries ($W = 2, 4$). They are not expected to appear in the 2d limit as there is no Fermi-surface nesting in the 2d band structure (shown in Fig. 1 (b)) at filling $\nu = 1/4$. In the 2d limit, the $U(1)$ gauge flux Φ also does not affect the parton Fermi surface. Therefore, we expect that the parton Fermi surface obtained from the mean-field ansatz Eq. (3) is stable in the 2d limit and provides a good candidate for the ground state of the $SU(4)$ -symmetric Kugel-Khomskii model Eq. (1) on the triangular lattice.

In real materials with spin and orbital degrees of freedom, one can only expect an approximate $SU(4)$ pseudospin symmetry. A small $SU(4)$ -symmetry-breaking perturbation is expected to split the 4-fold degeneracy of the 2d parton Fermi surface. A more comprehensive investigation of the stability of the parton Fermi surface to $SU(4)$ -symmetry-breaking perturbations and other non-Kugel-Khomskii-type interactions will be left for future studies.

Acknowledgments

This research is funded in part by the Gordon and Betty Moore Foundation through Grant GBMF8690 to UCSB to support the work of A.K. C.X. is supported by NSF Grant No. DMR-1920434, the David and Lucile Packard Foundation, and the Simons Foundation. Use was made of the computational facilities administered by the Center for Scientific Computing at the CNSI and MRL (an NSF MRSEC; DMR-1720256) and purchased through NSF CNS-1725797.

-
- [1] For recent reviews, see Refs. 45–48.
- [2] O. I. Motrunich and M. P. A. Fisher, Phys. Rev. B **75**, 235116 (2007).
- [3] D. N. Sheng, O. I. Motrunich, S. Trebst, E. Gull, and M. P. A. Fisher, Phys. Rev. B **78**, 054520 (2008).
- [4] D. N. Sheng, O. I. Motrunich, and M. P. A. Fisher, Phys. Rev. B **79**, 205112 (2009).
- [5] M. S. Block, R. V. Mishmash, R. K. Kaul, D. N. Sheng, O. I. Motrunich, and M. P. A. Fisher, Phys. Rev. Lett. **106**, 046402 (2011).
- [6] M. S. Block, D. N. Sheng, O. I. Motrunich, and M. P. A. Fisher, Phys. Rev. Lett. **106**, 157202 (2011), URL <http://link.aps.org/doi/10.1103/PhysRevLett.106.157202>.
- [7] R. V. Mishmash, M. S. Block, R. K. Kaul, D. N. Sheng, O. I. Motrunich, and M. P. A. Fisher, Phys. Rev. B **84**, 245127 (2011).
- [8] H.-C. Jiang, M. S. Block, R. V. Mishmash, J. R. Garrison, D. N. Sheng, O. I. Motrunich, and M. P. A. Fisher, Nature **493**, 39 (2013), URL <http://dx.doi.org/10.1038/nature11732>.
- [9] W.-Y. He, X. Y. Xu, G. Chen, K. T. Law, and P. A. Lee, Phys. Rev. Lett. **121**, 046401 (2018), URL <https://link.aps.org/doi/10.1103/PhysRevLett.121.046401>.
- [10] R. G. Pereira and S. Bieri, SciPost Phys. **4**, 004 (2017).
- [11] B. Bauer, B. P. Keller, S. Trebst, and A. W. W. Ludwig, Phys. Rev. B **99**, 035155 (2019), URL <https://link.aps.org/doi/10.1103/PhysRevB.99.035155>.
- [12] C. Hickey and S. Trebst, Nature communications **10**, 530 (2019).
- [13] N. D. Patel and N. Trivedi, Proceedings of the National Academy of Sciences **116**, 12199 (2019).
- [14] Y.-F. Jiang, T. P. Devereaux, and H.-C. Jiang, arXiv preprint arXiv:1901.09131 (2019).
- [15] N. Read and S. Sachdev, Nuclear Physics B **316**, 609 (1989), ISSN 0550-3213, URL <http://www.sciencedirect.com/science/article/pii/0550321389900618>.
- [16] S. Sachdev, Phys. Rev. B **45**, 12377 (1992), URL <https://link.aps.org/doi/10.1103/PhysRevB.45.12377>.
- [17] N. Read and S. Sachdev, Phys. Rev. Lett. **66**, 1773 (1991), URL <http://link.aps.org/doi/10.1103/PhysRevLett.66.1773>.
- [18] N. Read and S. Sachdev, Phys. Rev. B **42**, 4568 (1990), URL <http://link.aps.org/doi/10.1103/PhysRevB.42.4568>.
- [19] N. Read and S. Sachdev, Phys. Rev. Lett. **62**, 1694 (1989), URL <http://link.aps.org/doi/10.1103/>

- PhysRevLett. **62**.1694.
- [20] D. S. Rokhsar, Phys. Rev. B **42**, 2526 (1990), URL <https://link.aps.org/doi/10.1103/PhysRevB.42.2526>.
- [21] K. Penc, M. Mambrini, P. Fazekas, and F. Mila, Phys. Rev. B **68**, 012408 (2003), URL <https://link.aps.org/doi/10.1103/PhysRevB.68.012408>.
- [22] P. Corboz, M. Lajkó, A. M. Läuchli, K. Penc, and F. Mila, Phys. Rev. X **2**, 041013 (2012), URL <https://link.aps.org/doi/10.1103/PhysRevX.2.041013>.
- [23] S. K. Pati, R. R. P. Singh, and D. I. Khomskii, Phys. Rev. Lett. **81**, 5406 (1998), URL <https://link.aps.org/doi/10.1103/PhysRevLett.81.5406>.
- [24] Y. Q. Li, M. Ma, D. N. Shi, and F. C. Zhang, Phys. Rev. Lett. **81**, 3527 (1998), URL <https://link.aps.org/doi/10.1103/PhysRevLett.81.3527>.
- [25] Y. Tokura and N. Nagaosa, Science **288**, 462 (2000), ISSN 0036-8075, <https://science.sciencemag.org/content/288/5465/462.full.pdf>, URL <https://science.sciencemag.org/content/288/5465/462>.
- [26] A. V. Gorshkov, M. Hermele, V. Gurarie, C. Xu, P. S. Julienne, J. Ye, P. Zoller, E. Demler, M. D. Lukin, and A. M. Rey, Nature Physics **6**, 289 (2009).
- [27] C. Wu, J.-p. Hu, and S.-c. Zhang, Phys. Rev. Lett. **91**, 186402 (2003), URL <https://link.aps.org/doi/10.1103/PhysRevLett.91.186402>.
- [28] C. Wu, Phys. Rev. Lett. **95**, 266404 (2005), URL <https://link.aps.org/doi/10.1103/PhysRevLett.95.266404>.
- [29] C. WU, Modern Physics Letters B **20**, 1707 (2006), <https://doi.org/10.1142/S0217984906012213>, URL <https://doi.org/10.1142/S0217984906012213>.
- [30] C. Xu and L. Balents, Phys. Rev. Lett. **121**, 087001 (2018), URL <https://link.aps.org/doi/10.1103/PhysRevLett.121.087001>.
- [31] H. C. Po, L. Zou, A. Vishwanath, and T. Senthil, Phys. Rev. X **8**, 031089 (2018), URL <https://link.aps.org/doi/10.1103/PhysRevX.8.031089>.
- [32] Y.-H. Zhang and T. Senthil, arXiv:1809.05110 (2018).
- [33] X.-C. Wu, A. Keselman, C.-M. Jian, K. A. Pawlak, and C. Xu, Phys. Rev. B **100**, 024421 (2019), URL <https://link.aps.org/doi/10.1103/PhysRevB.100.024421>.
- [34] C. Schrade and L. Fu, Phys. Rev. B **100**, 035413 (2019), URL <https://link.aps.org/doi/10.1103/PhysRevB.100.035413>.
- [35] G. Chen, L. Jiang, S. Wu, B. Lyu, H. Li, B. L. Chittari, K. Watanabe, T. Taniguchi, Z. Shi, J. Jung, et al., Nature Physics **15**, 237 (2019).
- [36] Y. Cao, V. Fatemi, A. Demir, S. Fang, S. L. Tomarken, J. Y. Luo, J. D. Sanchez-Yamagishi, K. Watanabe, T. Taniguchi, E. Kaxiras, et al., Nature **556**, 80 (2018).
- [37] M. Yankowitz, S. Chen, H. Polshyn, Y. Zhang, K. Watanabe, T. Taniguchi, D. Graf, A. F. Young, and C. R. Dean, Science **363**, 1059 (2019), ISSN 0036-8075, <http://science.sciencemag.org/content/363/6431/1059.full.pdf>, URL <http://science.sciencemag.org/content/363/6431/1059>.
- [38] S. R. White, Phys. Rev. Lett. **69**, 2863 (1992).
- [39] U. Schollwöck, Rev. Mod. Phys. **77**, 259 (2005).
- [40] K. I. Kugel and D. I. Khomski, Soviet Physics Uspekhi **25**, 231 (1982), URL <https://doi.org/10.1070/2Fpu1982v025n04abeh004537>.
- [41] See Supplementary Material.
- [42] I. Affleck and E. H. Lieb, Letters in Mathematical Physics **12**, 57 (1986), ISSN 1573-0530, URL <https://doi.org/10.1007/BF00400304>.
- [43] ITensor Library, <http://itensor.org/>.
- [44] M. van den Bossche, P. Azaria, P. Lecheminant, and F. Mila, Phys. Rev. Lett. **86**, 4124 (2001), URL <https://link.aps.org/doi/10.1103/PhysRevLett.86.4124>.
- [45] L. Savary and L. Balents, Reports on Progress in Physics **80**, 016502 (2017).
- [46] Y. Zhou, K. Kanoda, and T.-K. Ng, Rev. Mod. Phys. **89**, 025003 (2017), URL <https://link.aps.org/doi/10.1103/RevModPhys.89.025003>.
- [47] J. Knolle and R. Moessner, Annual Review of Condensed Matter Physics **10**, 451 (2019), <https://doi.org/10.1146/annurev-conmatphys-031218-013401>, URL <https://doi.org/10.1146/annurev-conmatphys-031218-013401>.
- [48] C. Broholm, R. Cava, S. Kivelson, D. Nocera, M. Norman, and T. Senthil, arXiv preprint arXiv:1905.07040 (2019).

Supplementary Material

S1. PARTON BAND STRUCTURE FOR QUASI-1D GEOMETRIES WITH $W = 2, 3, 4$

In the main text, we focused on the 1d parton band structure with $\Phi = 0$ for $W = 2$, and $\Phi = \pi$ for $W = 3, 4$. Here, for completeness, we present the band structure for the complementary choice of Φ for each W (see Fig. S1). Comparing the two possible scenarios for each W , we see that the Φ s discussed in the main text have less partially occupied bands, and therefore, we expect them to be more stable. In addition, we find that that the complimentary choices of Φ are not compatible with the DMRG study, even if symmetry-allowed interactions are considered.

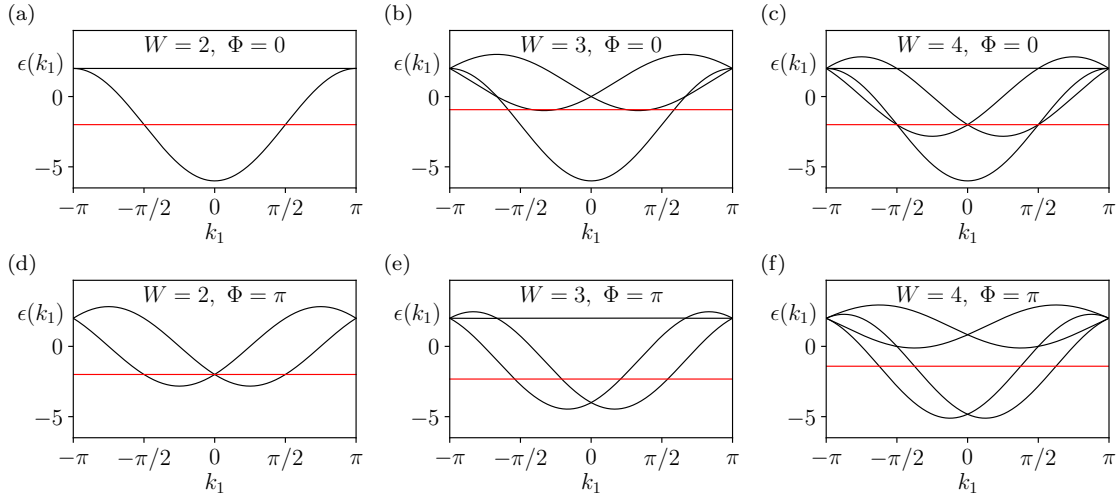


FIG. S1: Parton mean-field band structure for $W = 2, 3, 4$ for $\Phi = 0$ (upper panel) and $\Phi = \pi$ (lower panel). The red line indicates the Fermi level.

S1.1. Fermi momenta in the quasi-1d geometries

The Fermi momenta can be calculated directly from the mean-field Hamiltonian in Eq. (3) of the main text. In all the cases we consider, these Fermi momenta are also completely fixed by the symmetries \mathcal{T} , \mathcal{C}_2 and \mathcal{M} which act on the two momenta $k_{1,2}$ as

$$\mathcal{T} : k_{1,2} \rightarrow -k_{1,2}, \quad \mathcal{C}_2 : k_{1,2} \rightarrow -k_{1,2}, \quad \mathcal{M} : k_1 \rightarrow -k_1 + k_2, \quad k_2 \rightarrow k_2. \quad (\text{S1})$$

For $W = 2$ with $\Phi = 0$, the single partially occupied band has $k_2 = 0$ (see Fig. S1 (a)). The parton filling constraint requires the two Fermi points to differ in their k_1 -values by π . Either symmetry \mathcal{T} , \mathcal{M} , or \mathcal{C}_2 maps the two Fermi points into each other and, therefore, fixes their values to be $\pm\pi/2$.

For $W = 3, 4$ with $\Phi = \pi$, the two bands that are (partially) occupied by the partons have crystal momenta $k_2 = \pm\pi/W$ (see Fig. S1 (e) and (f)). They transform into each other under the time-reversal symmetry \mathcal{T} or \mathcal{C}_2 . The mirror symmetry \mathcal{M} preserves k_2 and, therefore, maps each partially occupied band to itself and interchanges the two Fermi points in each band. Taking the parton filling constraint into account, we conclude that the four Fermi momenta in the case of $W = 3, 4$ are fixed to be at $\pm\pi/(2W) \pm \pi W/8$.

This symmetry-based analysis ensures that the values of the Fermi momenta, in all the cases we focus on, are stable against small deformations to the mean-field ansatz Eq. (3).

S2. UMKLAPP INTERACTIONS FOR THE QUASI-1D GEOMETRIES WITH $W = 2$ AND $W = 4$

S2.1. Quasi-1d geometry with $W = 2$

As explained in the main text, the parton mean-field ansatz (including the coupling to U(1) gauge field) yields the $N_f = 4$ QED₂ (or equivalently the SU(4)₁ CFT) description of the quasi-1d geometry with $W = 2$:

$$\mathcal{L}_{\text{QED}, W=2} = \sum_{m=1}^4 \left[\psi_{L,m}^\dagger (i\partial_0 - a_0 - i\partial_1 + a_1) \psi_{L,m} + \psi_{R,m}^\dagger (i\partial_0 - a_0 + i\partial_1 - a_1) \psi_{R,m} \right]. \quad (\text{S2})$$

The Umklapp interaction in Eq. (5) of the main text can be rewritten as

$$\mathcal{L}_{W=2, \Phi=0}^{\text{int}} = \left(\sum_m \psi_{L,m}^\dagger \psi_{R,m} \right)^2 + h.c. = \frac{1}{2} \sum_{\alpha=1}^6 \left(\sum_{m_1, m_2=1}^4 \psi_{L, m_1}^\dagger M_{m_1 m_2}^\alpha \psi_{L, m_2}^\dagger \right) \left(\sum_{m_3, m_4=1}^4 \psi_{R, m_3} M_{m_3 m_4}^\alpha \psi_{R, m_4} \right) + h.c., \quad (\text{S3})$$

where M^α ($\alpha = 1, 2, \dots, 6$) are 4×4 matrices:

$$\begin{aligned} M^1 &= \begin{pmatrix} 0 & -i & 0 & 0 \\ i & 0 & 0 & 0 \\ 0 & 0 & 0 & 0 \\ 0 & 0 & 0 & 0 \end{pmatrix}, & M^2 &= \begin{pmatrix} 0 & 0 & -i & 0 \\ 0 & 0 & 0 & 0 \\ i & 0 & 0 & 0 \\ 0 & 0 & 0 & 0 \end{pmatrix}, & M^3 &= \begin{pmatrix} 0 & 0 & 0 & -i \\ 0 & 0 & 0 & 0 \\ 0 & 0 & 0 & 0 \\ i & 0 & 0 & 0 \end{pmatrix}, \\ M^4 &= \begin{pmatrix} 0 & 0 & 0 & 0 \\ 0 & 0 & -i & 0 \\ 0 & i & 0 & 0 \\ 0 & 0 & 0 & 0 \end{pmatrix}, & M^5 &= \begin{pmatrix} 0 & 0 & 0 & 0 \\ 0 & 0 & 0 & -i \\ 0 & 0 & 0 & 0 \\ 0 & i & 0 & 0 \end{pmatrix}, & M^6 &= \begin{pmatrix} 0 & 0 & 0 & 0 \\ 0 & 0 & 0 & 0 \\ 0 & 0 & 0 & -i \\ 0 & 0 & i & 0 \end{pmatrix}. \end{aligned} \quad (\text{S4})$$

Under the SU(4) pseudospin rotation, the 6 matrices M^α transform as the 6-dimensional representation of SU(4) (i.e. the vector representation of SO(6)). The $N_f = 4$ QED₂ can be viewed as a realization of the CFT coset construction $\text{SU}(4)_1 = \text{U}(4)_1 / \text{U}(1)_4$ where the $\text{U}(4)_1$ simply corresponds to a 4-component massless Dirac fermion without coupling to the U(1) gauge field. From this perspective, the field $\left(\sum_{m, m'=1}^4 \psi_{L,m}^\dagger M_{mm'}^\alpha \psi_{L,b}^\dagger \right)$ can be viewed as creating a primary field carrying the 6-dimensional representation of SU(4) in the left-moving sector of the SU(4)₁ CFT while its gauge charge under U(1) is “quotient” out by U(1)₄ in the coset-construction language. A similar reasoning applies to the field $\left(\sum_{m, m'=1}^4 \psi_{R,m}^\dagger M_{mm'}^\alpha \psi_{R,b}^\dagger \right)$. Therefore, as mentioned in the main text, we can interpret the Umklapp interaction Eq. (5) as the back-scattering between left-moving and right-moving primary fields in the SU(4)₁ CFT, both carrying the 6-dimensional representation of SU(4).

As we explained in the main text, the Umklapp interaction has scaling dimension 1 and, hence, is a relevant perturbation in the SU(4)₁ CFT. As it runs strong under the renormalization-group flow, the system can enter a phase where the field $\left(\sum_{m=1}^4 \psi_{L,m}^\dagger \psi_{R,m} \right)$ condenses. In this condensate, the Umklapp interaction effectively generates the following mass term for the Dirac fermions:

$$\mathcal{L}_{\text{mass}, W=2} = \phi \sum_{m=1}^4 \psi_{L,m}^\dagger \psi_{R,m} + \phi^* \sum_{m=1}^4 \psi_{R,m}^\dagger \psi_{L,m}, \quad (\text{S5})$$

where the complex number ϕ is essentially the (non-zero) vacuum expectation $\langle \sum_{m=1}^4 \psi_{L,m}^\dagger \psi_{R,m} \rangle$. This mass term gaps out all the low-energy excitations in the SU(4)₁ and spontaneously breaks the T_1 -translation symmetry with a doubled unit cell. This mass term still respects the SU(4)-pseudospin-rotation symmetry and the TR symmetry \mathcal{T} . When ϕ is not purely real, the mirror symmetry \mathcal{M} and the rotation symmetry C_2 are also spontaneously broken. Indeed, the DMRG results for $W = 2$ (shown in Fig. 3 (b) of the main text) do exhibit, in addition to the spontaneous breaking of T_1 , the breaking of both symmetries \mathcal{M} and C_2 .

S2.2. Quasi-1d geometry with $W = 4$

For the quasi-1d geometry with $W = 4$, the parton mean-field ansatz (including the coupling to $U(1)$ gauge field) yields the $N_f = 8$ QED₂ (or equivalently the $SU(8)_1$ CFT):

$$\mathcal{L}_{\text{QED},W=4} = \sum_{m=1}^4 \sum_{n=1}^2 \left[\psi_{L,n,m}^\dagger (i\partial_0 - a_0 - i\partial_1 + a_1) \psi_{L,n,m} + \psi_{R,n,m}^\dagger (i\partial_0 - a_0 + i\partial_1 - a_1) \psi_{R,n,m} \right], \quad (\text{S6})$$

where the 4-fold pseudospin index m and the 2-fold band index n together form the index for the fundamental representation of $SU(8)$ in the $SU(8)_1$ CFT. The Umklapp interactions

$$\left(\sum_{m=1}^4 \psi_{L,n,m}^\dagger \psi_{R,n,m} \right) \left(\sum_{m'=1}^4 \psi_{L,n',m'}^\dagger \psi_{R,n',m'} \right) + h.c., \quad (\text{S7})$$

with $n, n' = 1, 2$ preserve all the symmetries of the model but not necessarily the full $SU(8)$ enhanced symmetry of the $SU(8)_1$ CFT. Nevertheless, we can use the knowledge of the $SU(8)_1$ CFT to analyze the scaling dimension of the Umklapp interactions. Via a similar rewriting as Eq. (S3) and via the coset construction $SU(8)_1 = U(8)_1/U(1)_8$, we can identify the Umklapp terms as the back-scattering between left-moving and right-moving primary fields in the $SU(8)_1$ CFT, both carrying the 28-dimensional representation of $SU(8)$.

As explained in the main text, all such Umklapp interactions have the scaling dimension $3/2$ and hence are relevant under the renormalization group. At low energy, the Umklapp terms can drive the system into a phase with non-zero vacuum expectation values of both fields $\left(\sum_{m=1}^4 \psi_{L,1,m}^\dagger \psi_{R,1,m} \right)$ and $\left(\sum_{m=1}^4 \psi_{L,2,m}^\dagger \psi_{R,2,m} \right)$. In this phase, the Umklapp interactions effectively generate the following mass terms for the Dirac fermions:

$$\mathcal{L}_{\text{mass},W=4} = \phi_1 \sum_{m=1}^4 \psi_{L,1,m}^\dagger \psi_{R,1,m} + \phi_1^* \sum_{m=1}^4 \psi_{R,1,m}^\dagger \psi_{L,1,m} + \phi_2 \sum_{m=1}^4 \psi_{L,2,m}^\dagger \psi_{R,2,m} + \phi_2^* \sum_{m=1}^4 \psi_{R,2,m}^\dagger \psi_{L,2,m}, \quad (\text{S8})$$

where the complex numbers $\phi_{1,2}$ are essentially the vacuum expectation values $\langle \sum_{m=1}^4 \psi_{L,1,m}^\dagger \psi_{R,1,m} \rangle$ and $\langle \sum_{m=1}^4 \psi_{L,2,m}^\dagger \psi_{R,2,m} \rangle$ respectively. These mass terms gap out all the low-energy excitations in the $SU(8)_1$ CFT and spontaneously breaks the T_1 -translation symmetry with a doubled unit cell. They still respect the $SU(4)$ -pseudospin-rotation symmetry. The TR symmetry \mathcal{T} requires $\phi_1 = \phi_2$. If either ϕ_1 or ϕ_2 is not purely real, the mirror symmetry \mathcal{M} and rotation symmetry C_2 are spontaneously broken as well. Indeed, the DMRG results for $W = 4$ (shown in Fig. 3 (d) of the main text) do exhibit, in addition to the spontaneous breaking of T_1 , the breaking of both symmetries \mathcal{M} and C_2 .

S3. GUTZWILLER PROJECTED WAVEFUNCTIONS

Starting from the mean-field ansatz, the single-occupancy constraint on each site can be implemented by means of a Gutzwiller projection. Correlations in the resulting state can be probed using Monte Carlo sampling of the projected wavefunction. In the following, we will show that for $W = 3$, the correlations obtained from the Gutzwiller-projected wavefunction are in good agreement with the correlations of the exact ground state, as obtained from DMRG. For $W = 2$ and $W = 4$, we find that the Gutzwiller state does not break translational symmetry. However, it exhibits dominant correlations consistent with the CFT prediction.

For $W = 3$, we calculate the static structure factor (see Eq. (7) in the main text) in the Gutzwiller-projected state and verify that the cusps in the structure factor remain at the same values of the momenta as for the mean-field ansatz. This can be seen in Fig. S2.

Turning now to $W = 2$ and $W = 4$, we observe a power-law decay of the correlations for both cases, thus suggesting that the system is described by a gapless field theory. In Fig. S3, we show that the exponents of the decay are consistent with $3/2$ for the case of $W = 2$ and $7/4$ for $W = 4$. As we explain below, these values are consistent with the field theory predictions discussed in the main manuscript in the absence of the relevant Umklapp interactions, which apparently are not captured on the level of Gutzwiller projection. Specifically, the two field theories are $SU(4)_1$ CFT for $W = 2$ and $SU(8)_1$ CFT for $W = 4$ in the absence of Umklapp interactions.

For the $W = 2$ case, we consider gapless $N_f = 4$ QED₂ or the $SU(4)_1$ CFT without Umklapp interactions. The parton decomposition Eq. 2 suggests that the $SU(4)$ pseudospin correlation function $\sum_\alpha \langle \mathcal{S}_i^\alpha \cdot \mathcal{S}_j^\alpha \rangle$ should share the same scaling exponent with the correlations function $\langle \sum_m \psi_{L,m}(x) \psi_{L,m}^\dagger(0) \rangle \langle \sum_{m'} \psi_{R,m'}^\dagger(x) \psi_{R,m'}(0) \rangle$ in the $SU(4)_1$

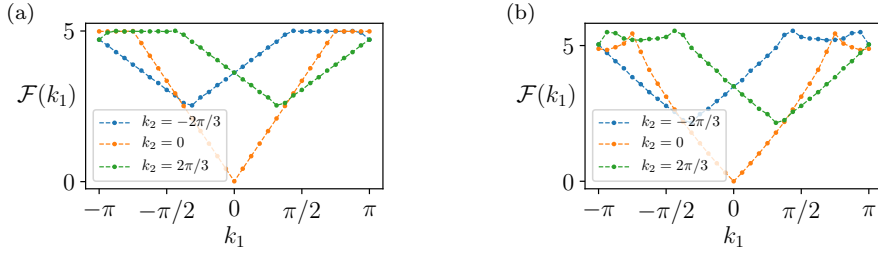


FIG. S2: Pseudospin structure factor obtained for a finite cylinder with $W = 3$ and length $L = 32$ with respect to a site in the middle of the system. (a) Non-interacting parton Fermi sea with $\Phi = \pi$; (b) Gutzwiller projection.

CFT. $\langle \sum_m \psi_{L,m}(x) \psi_{L,m}^\dagger(0) \rangle$ corresponds to the correlator of the left-moving primary field carrying the fundamental representation of $SU(4)$ which scales as $\sim |x|^{-\frac{3}{4}}$. Similarly, its right-moving counterpart $\langle \sum_{m'} \psi_{R,m'}^\dagger(x) \psi_{R,m'}(0) \rangle$ also scales as $\sim |x|^{-\frac{3}{4}}$. Therefore, based on the $SU(4)_1$ CFT, we expect the scaling $\sum_\alpha \langle \mathcal{S}_i^\alpha \cdot \mathcal{S}_j^\alpha \rangle \sim |x_i - x_j|^{-\frac{3}{2}}$ which is in agreement with the result for the Gutzwiller projected state shown in Fig. S3(a). Here, $|x_i - x_j|$ denote the distance between site i and j in the T_1 direction. In the parton band structure with $\Phi = 0$ for $W = 2$, the two Fermi points differ in their k_1 -values by π . We therefore expect a “2-site-periodic” modulation on top of the power-law decay in the $SU(4)$ -pseudospin correlation function, which is indeed observed in Fig. S3(a).

For the $W = 4$ case, we expect that the state is described by the gapless $N_f = 8$ QED₂ or the $SU(8)_1$ CFT without Umklapp interactions. The $SU(4)$ -pseudospin correlation function $\sum_\alpha \langle \mathcal{S}_i^\alpha \cdot \mathcal{S}_j^\alpha \rangle$ should now share the same scaling exponent with the correlations function $\langle \sum_m \psi_{L,m}(x) \psi_{L,m}^\dagger(0) \rangle \langle \sum_{m'} \psi_{R,m'}^\dagger(x) \psi_{R,m'}(0) \rangle$ in the $SU(8)_1$ CFT. $\langle \sum_m \psi_{L,m}(x) \psi_{L,m}^\dagger(0) \rangle$ corresponds to the correlator of the left-moving primary field carrying the fundamental representation of $SU(8)$ which scales as $\sim |x|^{-\frac{7}{8}}$. Similarly, its right-moving counterpart $\langle \sum_{m'} \psi_{R,m'}^\dagger(x) \psi_{R,m'}(0) \rangle$ also scales as $\sim |x|^{-\frac{7}{8}}$. Therefore, based on the $SU(8)_1$ CFT, we expect the scaling $\sum_\alpha \langle \mathcal{S}_i^\alpha \cdot \mathcal{S}_j^\alpha \rangle \sim |x_i - x_j|^{-\frac{7}{4}}$ which is in agreement with the result for the Gutzwiller projected state shown in Fig. S3(b). In the parton band structure with $\Phi = \pi$ for $W = 4$, the pairwise differences of the four Fermi points in their k_1 -values are commensurate to an 8-site unit cell along T_1 direction. We therefore expect an “8-site-periodic” modulation on top of the power-law decay in the $SU(4)$ -pseudospin correlation function, which is indeed observed in Fig. S3(b).

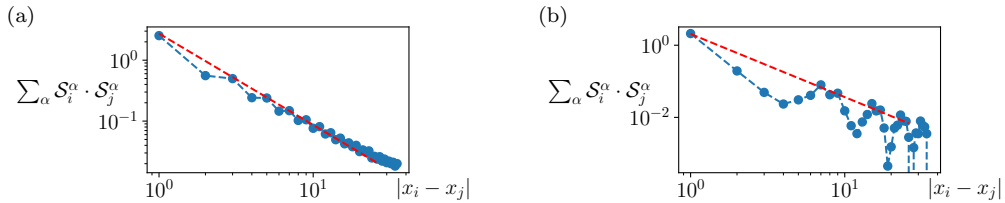


FIG. S3: Real space pseudospin correlations for the Gutzwiller projected wavefunctions in a system with periodic boundary conditions, length $L = 110$ and circumference $W = 2$ in (a) and $W = 4$ in (b). Red dashed lines corresponds to the exponents expected from the CFT, i.e. $3/2$ in (a) and $7/4$ in (b).

S4. ADDITIONAL DMRG RESULTS

S4.1. Energy extrapolation with truncation error for $W = 3$

To obtain a more accurate estimate for the gap for cylinders of circumference $W = 3$, we first extrapolate the energy in each quantum-numbers sector down to zero truncated weight. The gap is then calculated by subtracting the extrapolated energies. In Fig. S4 we show an example of the extrapolation procedure for a cylinder of length $L = 32$.

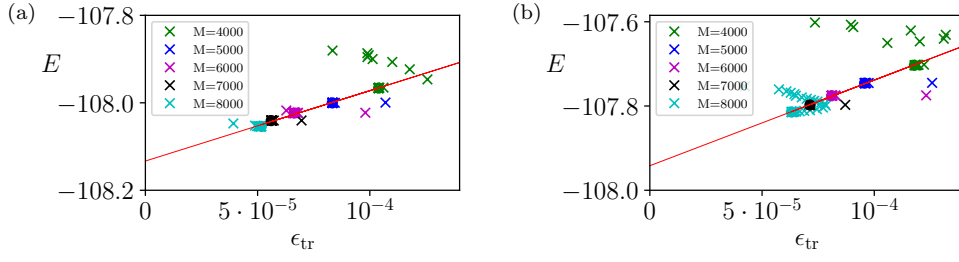


FIG. S4: Energy extrapolation with truncated weight for a cylinder of circumference $W = 3$ and length $L = 32$ (a) in the $(S^z, V^z, S^z V^z) = (0, 0, 0)$ sector and (b) in the $(S^z, V^z, S^z V^z) = (1, 0, -1/2)$ sector. Each cross on the plot corresponds to the energy, E , and truncated weight, ϵ_{tr} , for a given DMRG sweep, with the color of the point indicating the maximal bond dimension M for that sweep. The last sweep at each bond dimension is indicated by a square of the same color. These points are the ones used for the linear extrapolation of the energy down to zero truncated weight (the red line).

S4.2. Breaking of translation invariance for $W = 4$

To rule out the possibility that the ground state obtained in DMRG is a superposition of two states with broken translation symmetry along the circumference (i.e. along T_2), we double the strength of the coupling on one of the vertical bonds on the first rung of the cylinder. We observe only a relatively small change in the expectation values of the bonds close to the perturbed bond, and a rapid decay of the difference away from it, as can be seen in Fig. S5.

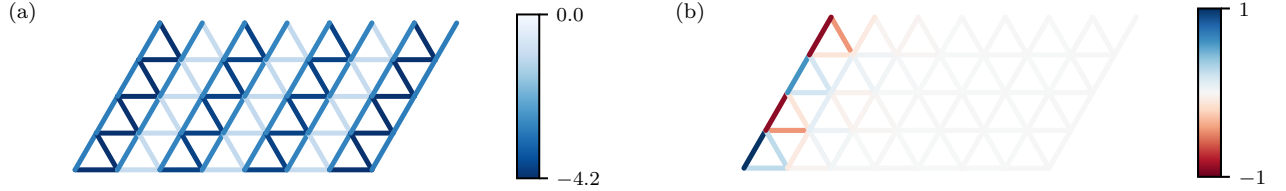


FIG. S5: (a) Expectation values of $\sum_{\alpha} S_i^{\alpha} \cdot S_j^{\alpha}$ for a cylinder of circumference $W = 4$ and length $L = 8$. (b) Difference in the bond expectation values upon doubling the strength of the coupling J on a vertical bond on the edge of the cylinder.